Journal of Power Sources 493 (2021) 229686

Contents lists available at ScienceDirect

Journal of Power Sources

journal homepage: www.elsevier.com/locate/jpowsour

Design and preparation of thin film gel polymer electrolyte for 3D Li-ion battery

Nurbol Tolganbek [a], Almagul Mentbayeva [a,*], Nurassyl Serik [a], Nursaule Batyrgali [a], Miras Naizakarayev [a], Kiyoshi Kanamura [c], Zhumabay Bakenov [a,b,**]

[a] Department of Chemical and Materials Engineering, Nazarbayev University, Nur-Sultan, Kazakhstan
[b] National Laboratory Astana, Nazarbayev University, Nur-Sultan, Kazakhstan
[c] Graduate School of Urban Environmental Sciences, Tokyo Metropolitan University, Tokyo, Japan

HIGHLIGHTS

- GPE of PEI and PAA were successfully coated onto Ni_3Sn_4 anode via LbL technique.
- An ultrathin GPE was evenly coated onto 3D structured anode surface.
- $(PEI/PAA)_n$ polymer coating improves the structural stability of the cell.
- 3D battery system demonstrated an excellent electrochemical performance.

GRAPHICAL ABSTRACT

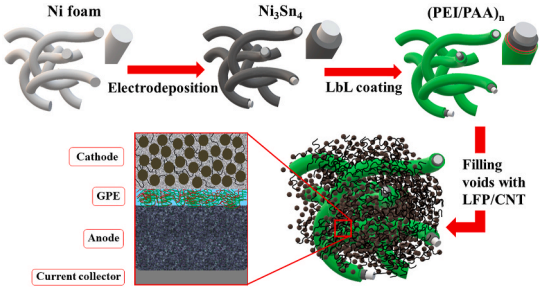

ARTICLE INFO

Keywords:
Lithium-ion battery (LIB)
3D battery
Anode
Gel electrolyte
Layer-by-layer assembly (LbL)
Ni–Sn alloy

ABSTRACT

Three-dimensional (3D) configuration of the battery provides a large active surface area of the electrodes to store and utilize more active material, enabling remarkable increase of capacity. Herein, we report on the development of a full 3D battery composed of Ni_3Sn_4 (Ni–Sn) alloy electrodeposited onto a nickel foam current collector to form a 3D anode, which was coated with a polymer electrolyte-separator film, and $LiFePO_4$/CNT cathode filled into the voids of the resulting 3D structure. An ultrathin polymer coating on the 3D anode was obtained via layer-by-layer technique. The X-ray diffraction investigations confirmed stability of the structure of the anode prior and after the polymer coating, while top and cross-section SEM images proved the uniformity of both the deposited 3D anode and the polymer coating on its surface. It was shown that a thin homogeneous layer of polymer can be obtained on 3D structured anode. This film effectively performed as a gel-like electrolyte in a full 3D battery. Cyclic voltammetry and charge-discharge tests exhibited stable electrochemical response and cyclability of the 3D battery. The prepared full 3D battery successfully operated at 0.1C rate and retained 90% of its initial capacity over 100 galvanostatic charge-discharge cycles.

* Corresponding author.
** Corresponding author. Department of Chemical and Materials Engineering, Nazarbayev University, Nur-Sultan, Kazakhstan.
E-mail addresses: almagul.mentbayeva@nu.edu.kz (A. Mentbayeva), Zbakenov@nu.edu.kz (Z. Bakenov).

https://doi.org/10.1016/j.jpowsour.2021.229686
Received 31 December 2020; Received in revised form 16 February 2021; Accepted 18 February 2021
Available online 28 February 2021

1. Introduction

Lithium-ion batteries (LIBs) have been widely used as power sources in most of portable electronics and electric vehicles devices as well as for stationary energy storage due to their long cycle life, high energy and power densities [1–4]. Recently a large number of research was dedicated to the increase of their power density in order to meet the performance requirements of some new advanced applications [5–7]. In order to achieve a high energy density of batteries, along with the development of new electrode materials, the electrode surface area could be maximized to enable high mass loading of electrochemically active material per unit area. Traditional planar or two-dimensional (2D) design of electrodes limits the active material mass loading within a 2D surface, and its further increase can be achieved by making thicker electrodes. However, the electrode thickness is restricted due to the following factors: i) risks of delamination of a thick electrode from current collector upon repeated charge-discharge; ii) slow lithium-ion diffusion/charge and mass transfer through a thick electrode layer; iii) in case of Li metal based battery, the lithium dendrite growth on electrode which leads to short circuiting [8,9]. These issues and demand to improve areal capacity of batteries lead to the concept of three-dimensional (3D) batteries [9], where a highly developed 3D surface permits deposition of a larger amount of the active material maintaining a lower thickness, i.e. eliminating the above mentioned problems related with a thick electrode [5]. Along with these benefits, a 3D structure can mitigate and compensate the volume variations of an electrode due to lithium insertion and extraction [10]. Furthermore, it was reported that lithium dendrite growth can be suppressed by using 3D metal based frameworks in lithium metal batteries [11–13]. Recently, Nurpeissova et al. reported on the Sn-based anodes on 3D current collector for lithium-ion batteries [14]. It was shown that the 3D design remarkably improves the battery performance due to the short Li^+ ions diffusion paths, high surface area and suppression of volume expansion of the electrode. Alternatively, electrical conductive low weight carbon based frameworks like carbon nanofibers [15], carbon nanotubes [16], and graphene [17,18] were used to obtain light and highly conductive 3D anodes with enhanced Li^+ ion conductivity. Moreover, the application of metal-carbon composites [19,20] and lithiophilic 3D frameworks [21,22] for preparation of 3D electrodes was reported, and the cells exhibited enhanced performance compared with the 'planar' counterparts. However, the design and structure of the batteries presented in those papers can be referred to as a "semi-3D" since three-dimensional active area of one electrode was connected with a counterpart electrode through a planar separator [23].

A few attempts to develop the batteries with 3D architecture of both electrodes were reported. Chamran et al. [24] proposed a 3D battery architecture based on interdigitated arrays of electrodeposited nickel and zinc, and liquid electrolyte. Moreover, other 3D architectures, such as honeycomb structured ceramic electrolyte with bidirectional pore arrangement filled with electrodes from both sides were investigated [25]. It was shown that the all-solid-state battery performs a discharge capacity of 32 μAh cm^{-2}. The capacity of electrodes and the cell was limited by small pore size and large wall thickness of the honeycomb pattern of solid electrolyte [25].

In the design of 3D batteries with a solid polymer electrolyte, mechanical properties of a separator/electrolyte and its conformal deposition are especially critical to ensure electrical separation of the electrodes. While being as thin as possible to decrease the Li^+ ion diffusion distance and enhance charge transfer, the electrolyte should be flexible to resist electrode expansion [26–28]. Several techniques for conformal deposition of polymer-based electrolytes onto 3D electrodes were investigated and reported. Many groups attempted to use electropolymerization to fabricate non-pin-hole solid polymer electrolytes for 3D batteries [29–31,36]. However, the electropolymerization technique has several drawbacks such as limited choice of electroactive monomers, the use of expensive working and counter electrodes such as platinum, gold and indium tin oxide (ITO) coated glass [32–34], and the limitations related with low conductivity of most of the electrodes preventing effective deposition of a polymer layer.

In this paper we present the fabrication and characterization of 3D full battery with Ni_3Sn_4 alloy anode on 3D metal substrate (Ni foam) and $LiFePO_4$ (LFP) cathode. The electrodes are separated by an ultrathin gel-like polymer electrolyte, which was fabricated using layer-by-layer (LbL) deposition method. LbL technique allowed the formation of a uniform and stable polymer (poly (ethylenimine)/poly (acrylic acid)) coating on a 3D anode with controllable nanometer range thickness, which was thermally cross-linked and loaded with liquid electrolyte in order to form Li-ion conductive gel-like polymer electrolyte (GPE). The 3D LFP/GPE/Ni_3Sn_4 cell demonstrated a stable cyclability up to 100 cycles with capacity retention of 90% and coulombic efficiency of 95%.

2. Materials and methods

2.1. Materials

Branched poly (ethylenimine) (PEI; MW = 750,000 by LS, 50 wt % in H_2O), poly (acrylic acid) (PAA; MW = 450,000), nickel foam (Goodfellow Inc., thickness 1.6 mm, porosity ≥ 95%), nickel (II) chloride ($NiCl_2{\cdot}6H_2O$, 99.9%), tin (II) chloride ($SnCl_2{\cdot}2H_2O$, 99.9%), potassium pyrophosphate ($K_4P_2O_7$, 97%), ammonium hydroxide (NH_4OH, 30%), glycine ($C_2H_5NO_2$, 99%), hydrogen peroxide solution (H_2O_2, 37%), single side polished silicon wafer and Trizma® buffer were purchased from Sigma-Aldrich and used as received. A commercial $LiFePO_4$ (LFP) starting powder and multi-walled carbon nanotubes (CNT, 95%, OD: 10–20 nm) supplied by Linyi Gelon LIB Co. Ltd. and US Research Nanomaterials, Inc. and consumed without any treatments.

2.2. Synthesis of anode

The Ni_3Sn_4 intermetallic alloy was electrodeposited on Ni foam to obtain 3D structured electrodes as reported in our previous work [14]. The electrodeposition was carried out in a two-electrode cell with Pt and Ni electrodes at 50 °C from a solution of 0.15 mol dm^{-3} $SnCl_2{\cdot}2H_2O$, 0.1 mol dm^{-3} $NiCl_2{\cdot}6H_2O$, 0.5 mol dm^{-3} $K_4P_2O_7$, 0.125 mol dm^{-3} glycine in DI water. The pH of solution was adjusted to 8 by NH_4OH. A constant current of 10 mA was provided by EL302RT Triple power supply (Aim Thurlby Thander Instruments Ltd.) for 10 min. After electrodeposition, the samples were washed with DI water and dried at 60 °C in a vacuum oven.

2.3. Gel polymer electrolyte formation

Before deposition of a polymer electrolyte, the surface of 3D anode was treated with 5% H_2O_2 aqueous solution and rinsed in DI water. For the deposition of the polymer electrolyte, the Ni–*Sn* electrodes and Si wafers were further immersed into 2 g dm^{-3} PEI solution with pH of 8.5 for 10 min, then rinsed with a buffer solution with the same pH. Then, the samples were immersed into 2 g dm^{-3} PAA solution of pH 5.0 for 10 min followed by rinsing by Trizma® buffer of pH 5.0. These steps were repeated *n* times and the coating was abbreviated as $(PEI/PAA)_n$, where *n* is the number of bilayers. Finally, the Ni–Sn samples with *n*-multilayered $(PEI/PAA)_n$ polymer electrolyte coating were washed with pure ethanol and dried.

2.4. Characterization techniques

Structure of electrodeposited Ni–Sn alloy was studied by X-ray diffraction (XRD, Rigaku SmartLab XRD system) equipped with Cu X-ray tube and D-Tex detector. Electrodeposited Ni_3Sn_4 sample and $(PEI/PAA)_n$ coated Ni_3Sn_4 surfaces were observed using a scanning electron microscope (SEM, FeSEM Auriga, (Crossbeam 540)). SEM with energy-dispersive spectroscopy (EDS) (JSM-IT 200) was used for elemental

mapping. The thickness of bilayers on silicon wafer was measured by a PHE – 101 Discrete Wavelength Ellipsometer (Angstrom Advanced).

2.5. Electrochemical investigation

Electrochemical measurements were conducted using CR2032-type coin cells assembled in an argon-filled glovebox (MasterLab, MBraun Inc.). For the lithium half-cell experiments, lithium foil was used as a counter and reference electrode. 1 M $LiPF_6$ solution in a mixture of ethylene carbonate/ethyl-methyl carbonate/dimethyl carbonate (EC/EMC/DC, 1:1:1 vol %) was consumed as an electrolyte. Celgard 2400 microporous polypropylene membrane was used as a separator. Cyclic voltammetry (CV) tests were performed on a VMP3 potentiostat/galvanostat (Bio-Logic Science Instr. Co.) at scanning rate of 0.1 mV s^{-1} between 0 and 1.4 V potential range. The lithium half-cell potentials are given with a reference to a lithium metal electrode.

3D full cells were also investigated in a CR2032-type coin cell configuration. In this case a Ni_3Sn_4 alloy served as both a negative/counter and reference electrode. Coated multilayers of $(PAA/PEI)_{30}$ on the alloy-deposited nickel foam served as a separator and electrolyte. Two drops of commercial LPF_6 liquid electrolyte was added on coated polymer multilayers to form a GPE. The LFP cathode slurry was prepared by dispersing LFP, carbon nanotubes (MWCNT) and polyvinylidene difluoride (PVdF) in a weight ratio of 6:3:1 in n-methyl-2-pyrrolidone (NMP). The slurry was injected into pores of a 3D alloy and polymer coated foam. Aluminum foil was used as a current collector for the cathode side. Fig. 1 schematically illustrates the preparation steps of the 3D battery. CV was carried out in a potential range of 0–3.2 V with a scanning rate of 0.1 mA s^{-1}. All electrochemical measurements were conducted at room temperature.

3. Results and discussion

The thin layer of Ni–Sn alloy anode was prepared by electroplating the alloy on a 3D structured Ni foam substrate, which served as a current collector in a battery assembled. The structure and composition of the deposited material was analyzed by XRD (Fig. 2, green line). The results illustrate that the electrodeposited alloy consists mainly of Ni_3Sn_4 phase with a hexagonal structure. The distinct peaks related to Ni_3Sn_4 appear at a range of 30–45° 2θ while there are also some weak peaks at 42° and 54° coming from the Ni_3Sn traces.

The major goal of this paper is to explore the capability of ultrathin LbL polyelectrolyte coating to act as a gel-like electrolyte and separator in 3D Li-ion cell, and assemble and test this battery. Therefore, the weak polybase and polyacid such as (poly (ethylenimine) (PEI) and poly

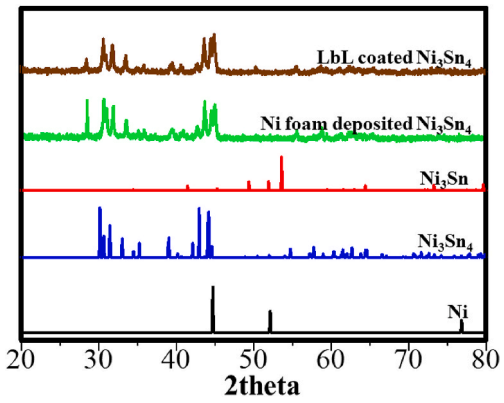

Fig. 2. XRD patterns of Ni (black), Ni_3Sn_4 (blue), Ni_3Sn (red) and electrodeposited (green) and polymer-coated Ni foams (brown). (For interpretation of the references to colour in this figure legend, the reader is referred to the Web version of this article.)

(acrylic acid) (PAA) were alternatively deposited from aqueous solutions onto the surface of 3D Ni–Sn alloy anode as schematically illustrated in Fig. S1. The $(PEI/PAA)_{10}$ coated Ni–Sn alloy also was studied by XRD (Fig. 2), which showed that the polymer coating does not affect the structure of the anode, which maintained the same XRD pattern as bare Ni_3Sn_4.

The growth of the $(PEI/PAA)_n$ coating was followed by ellipsometry measurements with polished silicon wafers substrates as illustrated in Fig. S3a. The results showed a thickness of 2 ± 1 nm of the first bilayer and a linear increase of it within initial ten bilayers, while exponential thickness growth was observed within further deposition steps. These results were highly reproducible upon precise control of deposition pH and agree well with the values reported in other works with the same system [35]. The thickness of 10 and 20 bilayers of LbL coating applied on the surface of Ni–Sn anode on 3D substrate was also estimated from a cross-sectional SEM image as 20 ± 3 nm and 60 ± 10 nm (Fig. 3a and b), which was consistent with the ellipsometric thickness. The cross-sectional Ni, Sn, C and O element mapping images of LbL coated 3D anode confirm the uniform depositions of Ni–Sn anode on Ni substrate and ultrathin polymer coating on top of it.

Although a uniform and complete coverage of the substrate (3D Ni–Sn alloy deposited Ni foam anode) was already achieved by depositing 10 bilayers of PEI/PAA, the thickness was not sufficient for stable electrochemical performance, but that of 20 bilayers was. At the same time the increase of bilayers number from 20 to 30 did not show any

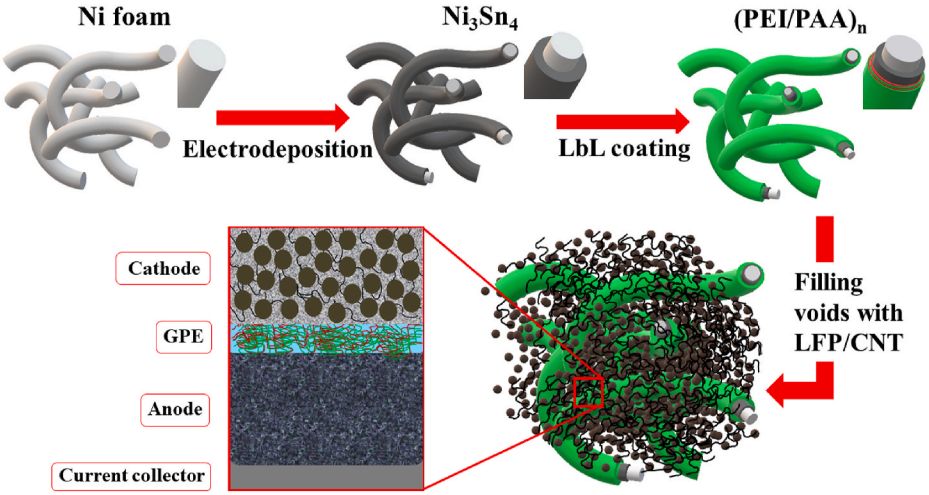

Fig. 1. Schematic illustration of 3D full battery fabrication and configuration.

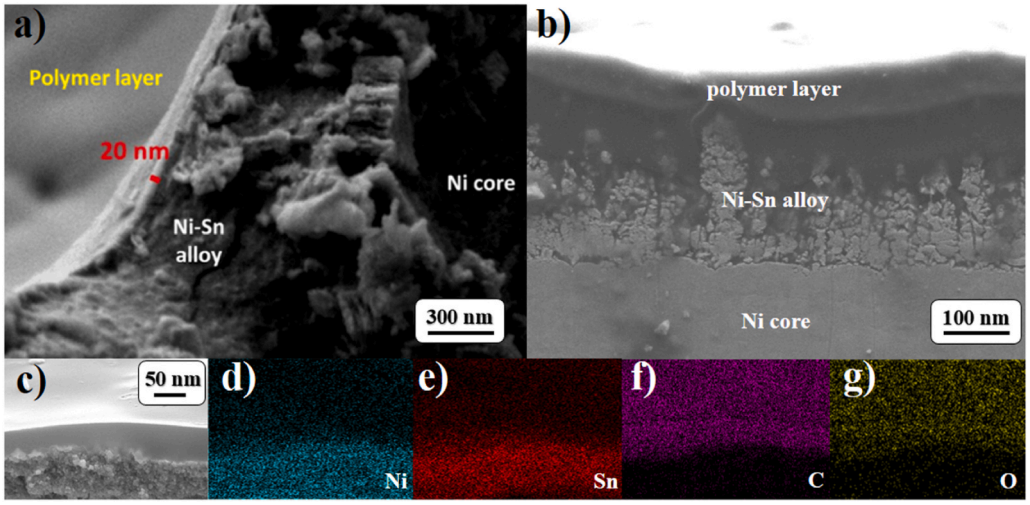

Fig. 3. Cross section SEM images of electrodeposited Ni–Sn alloy on Ni foam and with $(PEI/PAA)_n$ of 10 (a) and 20 bilayers (b), and cross-sectional EDS elemental mapping of Ni–Sn alloy/$(PEI/PAA)_n$ (c–g).

noticeable difference in cyclic voltammetry response (Fig. S3b). In order to ensure an effective electrical insulation and mechanical stability of the coating, 30 layers of PEI/PAA were applied and used for further studies. Fig. 4 depicts SEM images of bare nickel foam, Ni–Sn deposited Ni foam, and the surface of $(PEI/PAA)_{30}$ coated Ni–Sn alloy. Fig. 4a and b are the captures of nickel foam with a smooth surface at different magnifications. The surface morphology of the Ni_3Sn_4 electrodeposited Ni foam sample (Fig. 4c and d) differs from the bare one (Fig. 4a and b), demonstrating homogeneous deposition of Ni–Sn alloy on the foam substrate. The aggregates of cauliflower shape can clearly be seen in the inset of Fig. 4d. Fig. 4e and f demonstrate the $(PEI/PAA)_{30}$ coated surface of Ni–Sn alloy. The change of the surface of the foam framework is clearly depicted as a matt-like coverage after the polymer LbL deposition (Fig. 4e). Rough surface of Ni_3Sn_4 has become smooth (Fig. 4d) with uniform polymer coating. It can be observed that the foam framework structure was ideally preserved upon electrodeposition and polymer coatings. The absence of any cracks or holes in the polymer coating is crucial for a safe operation of the battery since the LbL polyelectrolyte coating loaded with 1 M $LiPF_6$ solution in EC/EMC/DC is supposed to act as both an electrolyte providing Li-ion conductance and a separator ensuring electrical insulation of electrodes from each other.

Since PEI and PAA are weak polyelectrolytes, in aqueous media the charge density of their molecules can be controlled by adjusting the acidity solutions. Therefore, LbL coating based on electrochemical interaction was grown from solutions with pH values close to pKa of the polymers, i.e. 8.5 and 5.0 for PEI (pK_b ~ 8.8) and PAA (pKa ~5.0), respectively (Fig. S1). In order to investigate the stability of formed polymer assembly in the electrolyte solution (1 M $LiPF_6$ in EC/EMC/DMC) with a high ionic strength, the $(PEI/PAA)_{30}$ layers were deposited on Si wafer substrates. It was followed by a thermal cross-linking at 130 °C for 1 h to covalently bond PAA and PEI layers through amine and carboxylic groups interaction [7] (Fig. S2). The samples with and without thermal cross-linking were challenged by immersing into the electrolyte solution for 12 h. SEM images of these samples before and after soaking into the electrolyte and rinsing with the corresponding solvent are shown in Fig. 5a–d. The surface of substrates remained the same in both cases. Thus, it can be assumed that the heat treatment of polymer coating is not essential but may be applied to further improve their stability. Additionally, in Fig. 5a a clear border between polymer coated substrate and scratched area can be seen. Fig. 5b–d illustrate the

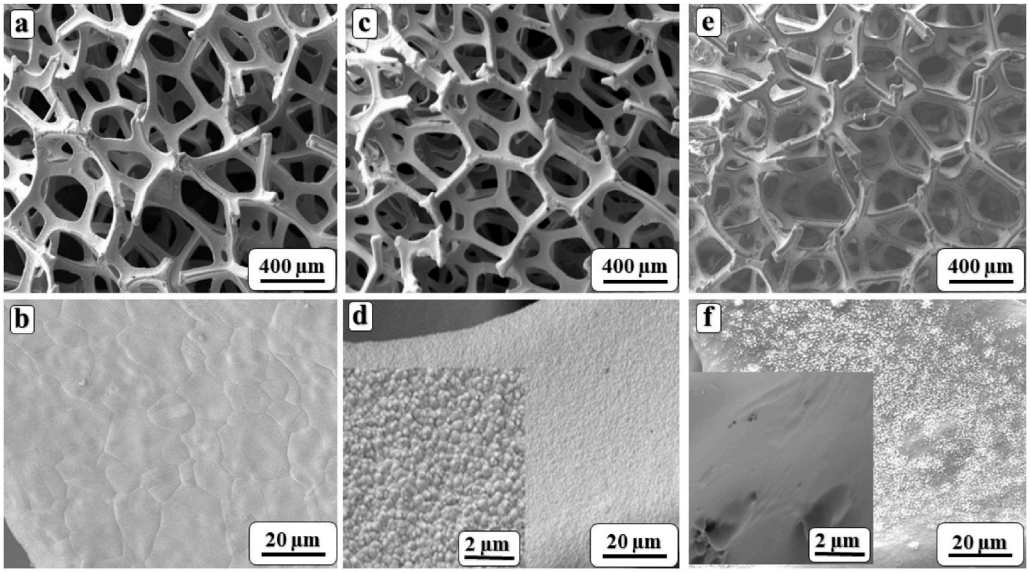

Fig. 4. SEM images of bare nickel foam (a,b), Ni_3Sn_4 anode electrodeposited sample (c,d) and (e,f) $(PEI/PAA)_{30}$ coated anode surface.

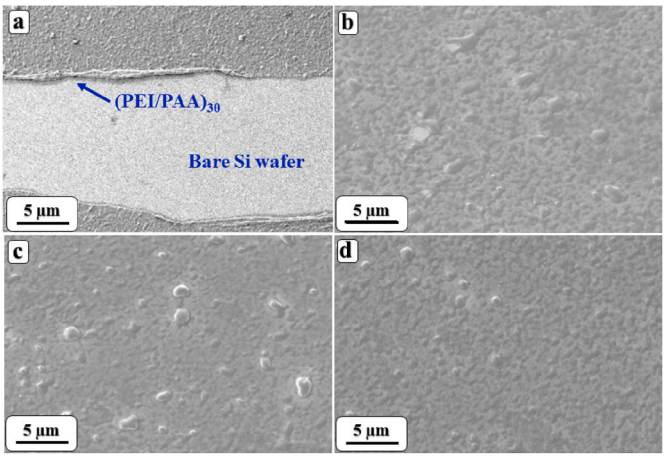

Fig. 5. SEM images of (a, b) polymer layer of $(PEI/PAA)_{30}$ on smooth substrate surface of Si wafer, and soaked in 1 M $LiPF_6$ in EC/EMC/DMC (c) before and (d) after heat treatment.

uniform coating of 30 bilayers of PEI/PAA on Si wafer without any cracks and inconsistencies. Along with the excellent stability in the electrolyte media and uniform coverage of the anode surface, the ultrathin $(PEI/PAA)_{30}$ coating, in contrast with common polymer separators, negligibly adds to the weight and volume of the battery and does not negatively affect its overall power density.

Electrochemical performance of the electrodeposited Ni_3Sn_4 alloy on Ni foam was tested using standard Li half-cells. A half-cell was assembled using Ni–Sn alloy as a working electrode and lithium metal as both reference and counting electrodes with a Celgard separator between the electrodes. Mass loading of the active material onto nickel foam substrates was in a range of 1.97–2.0 mg cm^{-2}. Cyclic voltammetry (CV) measurements were conducted at a scanning rate of 0.1 mV s^{-1} within a potential range of 0–1.5 V, and the results are shown in Fig. 6. Three cathodic, and four anodic peaks in the second cycle were assigned to a multistep redox process of alloying and dealloying of Sn and Ni_3Sn_4 phases with lithium ions. A cathodic peak at 0.65 V corresponds to the formation of Sn–Li, while two overlapping main peaks at around 0.26–0.35 V are attributed to a stepwise evolution of $Li_{22}Sn_5$. The observed CV responses of the alloy anode correlates with those in previously reported works [37]. It should be noted that the first cycle remarkably differs from the consecutive cycles, which can be explained by a development of a solid electrolyte interface (SEI) layer within the initial cycle. Similar patterns can be observed for a half-cell that was assembled with LbL coated 3D Ni–Sn alloy electrode (Fig. 6b). This demonstrates that the polymer coating does not affect the electrochemistry of the system within the working potential range of the active material, and acts as GPE/separator without side reactions and alteration of the chemistry of the electrode. While ionic conductivity measurement of GPE with blocking and non-blocking electrodes could not be conducted due to the tool's inability to test nanoscale coatings, the EIS measurement was performed in a cell with Ni–Sn alloy and lithium metal. The spectra in Fig. S4 clearly represents that the cell with an ultrathin gel-like polymer electrolyte coated Ni–Sn anode has significantly lower resistivity compared to the one with liquid electrolyte and Celgard separator.

Galvanostatic charge and discharge profiles of LFP cathode and Ni–Sn alloy anode with lithium metal were obtained and the results are demonstrate in Fig. S4. The electrodes have performed stable with a specific capacity of ~160 and ~995 mAh g^{-1} at 0.1C for LFP and Ni_3Sn_4, respectively. Further, the 3D full battery was constructed using $(PEI/PAA)_{30}$ coated Ni–Sn alloy onto Ni foam substrate as a negative electrode and $LiFePO_4$ mixed with CNT as a positive electrode. The cell with 10 and 20 bilayers did not demonstrated any stable electrochemical performance. The cathode was filled into the free voids of LbL coated anode as illustrated in Fig. 1. The CV tests were carried out at a scanning rate of 0.5 mV s^{-1} within a potential range of 1–4 V. A cyclic voltammogram of 3D full cell is presented in Fig. 6c demonstrating a characteristic CV plot of a $LiFePO_4$ Li-ion cell. The cell exhibits one pair of reversible CV peaks, a broad peak at around 3.45 V reflecting the delithiation of LFP and a corresponding reversible lithiation process occurring at 2.70 V.

The galvanostatic charge and discharge of the 3D full cell was run within a cutoff range of 1.0 V–3.6 V, and the corresponding potential profiles and cycle performance are depicted in Fig. 7 a, b. It can be seen that the initial discharge capacity of the battery was 134 mAh g^{-1} at 0.1C. The discharge capacity increases up to 159 mAh g^{-1} within further cycles. It remained at 143 mAh g^{-1} after the 100th cycle with a capacity retention of about 90%. Coulombic efficiency of the cell increased over the initial cycles and stabilized at 95% beginning from the 10th cycle. Such tendency in the coulombic efficiency could be due to the formation of a solid electrolyte interface (SEI) layer during the initial cycles, which consumed additional electrons. In the consecutive cycles such side reactions weakening and the coulombic efficiency of 95% was achieved. A rate step-progressive tests of the cells have been carried out as presented in Fig. 7c. The cells were galvanostatically cycled at a current density of 0.1C for 5 cycles, and then the current density was gradually increased up to 5C. Stable discharge capacities of 153, 131, 116 75, 46 mAh g^{-1} were obtained for LFP at current densities of 0.2, 0.5, 1, 2 and 5C, respectively. After five cycles at 5C rate, the cell restored the discharge capacity of ~145 mAh g^{-1} for further cycles at 0.1C. Taking into account a small resistivity of the ultrathin gel-like polymer electrolyte layer, it is likely that electrodes conductivity is a key factor in achieving high rate performance of the 3D cell.

Having the lower coulombic efficiency value in the initial cycles further described by combinational measurements of electrochemical impedance spectroscopy and glavanostatic charge and discharge

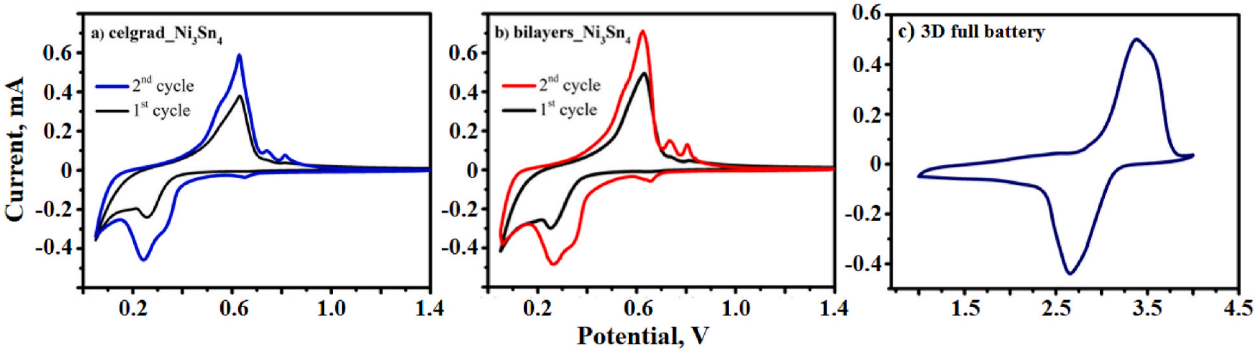

Fig. 6. CV profiles of bare (a) and $(PEI/PAA)_{30}$ coated Ni_3Sn_4 alloy in Li half cell (b) at a scanning rate 0.1 mV s^{-1}, and CV profile of $Ni_3Sn_4|(PEI/PAA)_{30}|$LFP 3D full cell (c) at a scanning rate 0.5 mV s^{-1}.

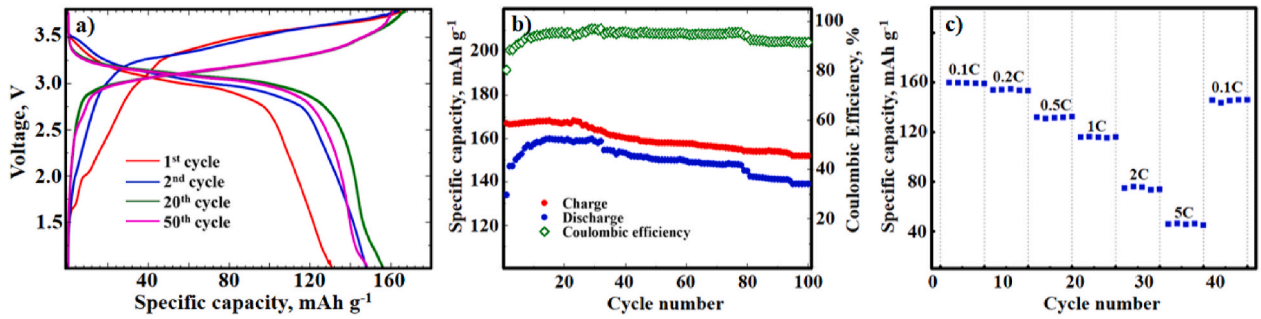

Fig. 7. Electrochemical performance of 3D full battery. Galvanostatic charge and discharge profile (a), cyclability and coulombic efficiency at 0.1C (b), rate capability (c).

analysis. The EIS of 3D full battery before and after galvanostatic charge and discharge examination is depicted in Fig. 8a.

The EIS of the fresh cell demonstrates the lowest charge transfer resistance, which abruptly escalates with initial cycles. The semicircle growth is due to the SEI formation, and further enlargement is explained by the pulverization of the alloy [38]. This process is extended for farther two cycles. The resistivity decreases starting from the 5th to 10th cycles and a little change was further observed due to the stabilized SEI layer [39].

To further explore the degradation mechanism of the battery, the cells were disassembled after 50 cycles of galvanostatic charge-discharge, and structural and morphological analysis of the LbL coated anode was performed. The XRD analysis of the cycled Ni_3Sn_4 anode showed that the crystalline structure of the material was not affected by repeated oxidation-reduction reactions (Fig. S6). Fig. 8b and c illustrate SEM images of fresh and cycled Ni–Sn alloy anodes on Ni foam without polymer layer, which distinctly show an appearance of considerable number of cracks after cycling of Ni–Sn alloy. SEM images of LbL coated Ni–Sn electrode before and after cycling are demonstrated in Fig. 8 d-j. As can be seen from Fig. 8d and e, the surface morphology of polymer coating has not changed after 50 cycles. SEM images from the cross-section view clearly exposed the established interphase boarder between anode and GPE after cycling (Fig. 8j), while before cycling it was smooth (Fig. 8f). Constant Li alloying and dealloying process slightly influenced on the interface between the polymer coating and the anode, while the coating itself remained complete and uniform without any cracks. It is likely that the ultrathin polymer coating improves the structural stability of the cell allowing to have better performance without any damage or delamination during the electrochemical tests.

This work demonstrates a successful design and operation of a 3D full lithium-ion cell by applying a layer-by-layer deposited thin polymer electrolyte film on a 3D anode with further filling the 3D cavities with a cathode. The LbL deposited polymer electrolyte effectively acts as a gel-like electrolyte and separator.

4. Conclusion

A full 3D lithium-ion cell Ni foam|Ni_3Sn_4|$(PEI/PAA)_{30}$|LFP was designed and successfully assembled via a simple route by electrodeposition of 3D Ni_3Sn_4 anode onto Ni foam, followed by a layer-by-layer deposition of a thin PEI/PAA polymer electrolyte on this 3D structure, and filling the positive electrode $LiFePO_4$ into its cavities. Layer-by-layer method was shown as an effective route to obtain a complete coating of a thin polymer electrolyte onto 3D Ni_3Sn_4 anode. The uniqueness of LbL as a technique capable of obtaining a thin polymer electrolyte layer on a 3D structure with a controllable thickness was confirmed by successful operation of the 3D battery. Along with the enhanced structural stability, the cell exhibited stable cycling and rate capability with high specific capacity and coulombic efficiency.

The capability of LbL to control the thickness of multilayer coating, which ensures enhanced lithium ion transport, makes this technique a considerable choice for future developments of advanced systems for energy storage. Along with this, the electrochemical and mechanical stability of such thin and lightweight electrolyte/separator enable an alternative choice of its application to increase a footprint energy density of electrodes.

CRediT authorship contribution statement

Nurbol Tolganbek: Methodology, Validation, Data curation, Writing – original draft. **Almagul Mentbayeva:** Conceptualization, Recourses, Writing – review & editing, Project administration. **Nurassyl**

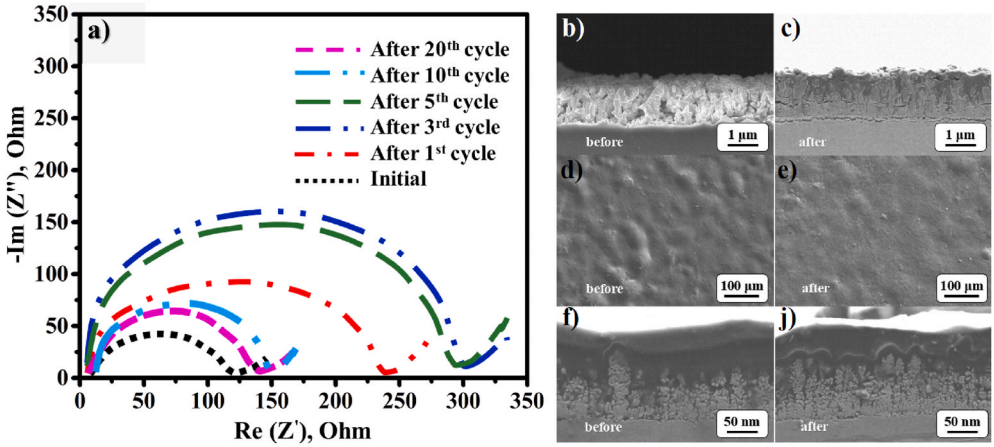

Fig. 8. EIS profiles of Ni_3Sn_4|$(PEI/PAA)_{30}$|LFP before and after 1st, 3rd, 5th, 10th and 20th cycles during galvanostatic charge and discharge process (a). Cross-section (b, c, f, j) and top (d, e) view SEM images of 3D battery system before and after 50 cycles of charge-discharge.

Serik: Data curation, Writing – original draft, Visualization. **Nursaule Batyrgali:** Validation, Writing – original draft, Investigation. **Miras Naizakarayev:** Data curation, Validation, Investigation. **Kiyoshi Kanamura:** Recourses, Writing – review & editing. **Zhumabay Bakenov:** Conceptualization, Writing – review & editing, Funding acquisition.

Declaration of competing interest

The authors declare that they have no known competing financial interests or personal relationships that could have appeared to influence the work reported in this paper.

Acknowledgment

This research was supported by the research grants #021220CRP0122 “Development of highly sensitive MOS based nano-film gas sensors” and #091019CRP2114 “Three-dimensional all solid state rechargeable batteries” from Nazarbayev University. Authors thank Core Facilities of Nazarbayev University for access to laboratory equipment.

Appendix A. Supplementary data

Supplementary data to this article can be found online at https://doi.org/10.1016/j.jpowsour.2021.229686.

References

[1] N. Liu, H. Wu, M.T. McDowell, Y. Yao, C. Wang, Y. Cui, A yolk-shell design for stabilized and scalable Li-ion battery alloy anodes, Nano Lett. 12 (2012) 3315–3321, https://doi.org/10.1021/nl3014814.
[2] D. Ahn, X. Xiao, Y. Li, A.K. Sachdev, H.W. Park, A. Yu, Z. Chen, Applying functionalized carbon nanotubes to enhance electrochemical performances of tin oxide composite electrodes for Li-ion battery, J. Power Sources 212 (2012) 66–72, https://doi.org/10.1016/j.jpowsour.2012.03.075.
[3] F.M. Hassan, Z. Chen, A. Yu, Z. Chen, X. Xiao, Sn/SnO2 embedded in mesoporous carbon nanocomposites as negative electrode for lithium ion batteries, Electrochim. Acta 87 (2013) 844–852, https://doi.org/10.1016/j.electacta.2012.09.015.
[4] J.Y. Liao, D. Higgins, G. Lui, V. Chabot, X. Xiao, Z. Chen, Multifunctional TiO2-C/MnO2 core-double-shell nanowire arrays as high-performance 3D electrodes for lithium ion batteries, Nano Lett. 13 (2013) 5467–5473, https://doi.org/10.1021/nl4030159.
[5] G.E. Blomgren, The development and future of lithium ion batteries, J. Electrochem. Soc. 164 (2017), https://doi.org/10.1149/2.0251701jes. A5019–A5025.
[6] S. Ferrari, M. Loveridge, S.D. Beattie, M. Jahn, R.J. Dashwood, R. Bhagat, Latest advances in the manufacturing of 3D rechargeable lithium microbatteries, J. Power Sources 286 (2015) 25–46, https://doi.org/10.1016/j.jpowsour.2015.03.133.
[7] A. Mentbayeva, S. Sukhishvili, M. Naizakarayev, N. Batyrgali, Electrochimica Acta Ultrathin clay-containing layer-by-layer separator coating enhances performance of lithium-sulfur batteries, Electrochim. Acta 366 (2021) 137454, https://doi.org/10.1016/j.electacta.2020.137454.
[8] C. Fongy, A.-C. Gaillot, S. Jouanneau, D. Guyomard, B. Lestriez, Ionic vs electronic power limitations and analysis of the fraction of wired grains in LiFePO[sub 4] composite electrodes, J. Electrochem. Soc. 157 (2010) A885, https://doi.org/10.1149/1.3432559.
[9] P.V. Braun, J. Cho, J.H. Pikul, W.P. King, H. Zhang, High power rechargeable batteries, Curr. Opin. Solid State Mater. Sci. 16 (2012) 186–198, https://doi.org/10.1016/j.cossms.2012.05.002.
[10] T.S. Arthur, D.J. Bates, N. Cirigliano, D.C. Johnson, P. Malati, J.M. Mosby, E. Perre, M.T. Rawls, A.L. Prieto, B. Dunn, Three-dimensional electrodes and battery architectures, MRS Bull. 36 (2011) 523–531, https://doi.org/10.1557/mrs.2011.156.
[11] C.P. Yang, Y.X. Yin, S.F. Zhang, N.W. Li, Y.G. Guo, Accommodating lithium into 3D current collectors with a submicron skeleton towards long-life lithium metal anodes, Nat. Commun. 6 (2015), https://doi.org/10.1038/ncomms9058.
[12] P. Zou, Y. Wang, S.W. Chiang, X. Wang, F. Kang, C. Yang, Directing lateral growth of lithium dendrites in micro-compartmented anode arrays for safe lithium metal batteries, Nat. Commun. 9 (2018), https://doi.org/10.1038/s41467-018-02888-8.
[13] H. Lee, J. Song, Y.J. Kim, J.K. Park, H.T. Kim, Structural modulation of lithium metal-electrolyte interface with three-dimensional metallic interlayer for high-performance lithium metal batteries, Sci. Rep. 6 (2016) 1–10, https://doi.org/10.1038/srep30830.
[14] A. Nurpeissova, A. Adi, A. Aishova, A. Mukanova, S.S. Kim, Z. Bakenov, Synergistic effect of 3D current collector structure and Ni inactive matrix on the electrochemical performances of Sn-based anodes for lithium-ion batteries, Mater. Today Energy. 16 (2020) 100397, https://doi.org/10.1016/j.mtener.2020.100397.
[15] X. Zhou, W. Huang, C. Shi, K. Wang, R. Zhang, J. Guo, Y. Wen, S. Zhang, Q. Wang, L. Huang, J. Li, X. Zhou, S. Sun, Enabling lithium-metal anode encapsulated in a 3D carbon skeleton with a superior rate performance and capacity retention in full cells, ACS Appl. Mater. Interfaces 10 (2018) 35296–35305, https://doi.org/10.1021/acsami.8b13506.
[16] J. Xiang, Y. Zhao, L. Yuan, C. Chen, Y. Shen, F. Hu, Z. Hao, J. Liu, B. Xu, Y. Huang, A strategy of selective and dendrite-free lithium deposition for lithium batteries, Nanomater. Energy 42 (2017) 262–268, https://doi.org/10.1016/j.nanoen.2017.10.065.
[17] D. Lin, Y. Liu, Z. Liang, H.W. Lee, J. Sun, H. Wang, K. Yan, J. Xie, Y. Cui, Layered reduced graphene oxide with nanoscale interlayer gaps as a stable host for lithium metal anodes, Nat. Nanotechnol. 11 (2016) 626–632, https://doi.org/10.1038/nnano.2016.32.
[18] R. Mukherjee, A.V. Thomas, D. Datta, E. Singh, J. Li, O. Eksik, V.B. Shenoy, N. Koratkar, Defect-induced plating of lithium metal within porous graphene networks, Nat. Commun. 5 (2014), https://doi.org/10.1038/ncomms4710.
[19] J. Pu, J. Li, Z. Shen, C. Zhong, J. Liu, H. Ma, J. Zhu, H. Zhang, P.V. Braun, Interlayer lithium plating in Au nanoparticles pillared reduced graphene oxide for lithium metal anodes, Adv. Funct. Mater. 28 (2018) 1–8, https://doi.org/10.1002/adfm.201804133.
[20] A.R.O. Raji, R. Villegas Salvatierra, N.D. Kim, X. Fan, Y. Li, G.A.L. Silva, J. Sha, J. M. Tour, Lithium batteries with nearly maximum metal storage, ACS Nano 11 (2017) 6362–6369, https://doi.org/10.1021/acsnano.7b02731.
[21] X.B. Cheng, T.Z. Hou, R. Zhang, H.J. Peng, C.Z. Zhao, J.Q. Huang, Q. Zhang, Dendrite-free lithium deposition induced by uniformly distributed lithium ions for efficient lithium metal batteries, Adv. Mater. 28 (2016) 2888–2895, https://doi.org/10.1002/adma.201506124.
[22] C. Niu, H. Pan, W. Xu, J. Xiao, J.G. Zhang, L. Luo, C. Wang, D. Mei, J. Meng, X. Wang, Z. Liu, L. Mai, J. Liu, Self-smoothing anode for achieving high-energy lithium metal batteries under realistic conditions, Nat. Nanotechnol. 14 (2019) 594–601, https://doi.org/10.1038/s41565-019-0427-9.
[23] M. Roberts, P. Johns, J. Owen, D. Brandell, K. Edstrom, G. El Enany, C. Guery, D. Golodnitsky, M. Lacey, C. Lecoeur, H. Mazor, E. Peled, E. Perre, M. M. Shaijumon, P. Simon, P.L. Taberna, 3D lithium ion batteries - from fundamentals to fabrication, J. Mater. Chem. 21 (2011) 9876–9890, https://doi.org/10.1039/c0jm04396f.
[24] F. Chamran, Y. Yeh, H.S. Min, B. Dunn, C.J. Kim, Fabrication of high-aspect-ratio electrode arrays for three-dimensional microbatteries, J. Microelectromechanical Syst. 16 (2007) 844–852, https://doi.org/10.1109/JMEMS.2007.901638.
[25] M. Kotobuki, Y. Suzuki, H. Munakata, K. Kanamura, Y. Sato, K. Yamamoto, T. Yoshida, Effect of sol composition on solid electrode/solid electrolyte interface for all-solid-state lithium ion battery, Electrochim. Acta 56 (2011) 1023–1029, https://doi.org/10.1016/j.electacta.2010.11.008.
[26] J.W. Long, B. Dunn, D.R. Rolison, H.S. White, Three-dimensional battery architectures, Chem. Rev. 104 (2004) 4463–4492, https://doi.org/10.1021/cr020740l.
[27] P.G. Bruce, B. Scrosati, J.M. Tarascon, Nanomaterials for rechargeable lithium batteries, Angew. Chem. Int. Ed. 47 (2008) 2930–2946, https://doi.org/10.1002/anie.200702505.
[28] R.C. Agrawal, G.P. Pandey, Solid polymer electrolytes: materials designing and all-solid-state battery applications: an overview, J. Phys. D Appl. Phys. 41 (2008), https://doi.org/10.1088/0022-3727/41/22/223001.
[29] N.S. Ergang, M.A. Fierke, Z. Wang, W.H. Smyrl, A. Stein, Fabrication of a fully infiltrated three-dimensional solid-state interpenetrating electrochemical cell, J. Electrochem. Soc. 154 (2007) A1135, https://doi.org/10.1149/1.2794288.
[30] G. El-Enany, M.J. Lacey, P.A. Johns, J.R. Owen, In situ growth of polymer electrolytes on lithium ion electrode surfaces, Electrochem. Commun. 11 (2009) 2320–2323, https://doi.org/10.1016/j.elecom.2009.10.019.
[31] C.P. Rhodes, J.W. Long, M.S. Doescher, B.M. Dening, D.R. Rolison, Charge insertion into hybrid nanoarchitectures: mesoporous manganese oxide coated with ultrathin poly(phenylene oxide), J. Non-Cryst. Solids 350 (2004) 73–79, https://doi.org/10.1016/j.jnoncrysol.2004.06.050.
[32] B.C. Venancio, C.A.R. Costa, S.A.S. Machado, A.J. Motheo, AFM study of the initial stages of polyaniline growth on ITO electrode, Electrochem. Commun. 3 (2001) 229–233, https://doi.org/10.1016/S1388-2481(01)00153-9.
[33] P.D. Gaikwad, D.J. Shirale, V.K. Gade, P.A. Savale, H.J. Kharat, K.P. Kakde, S. S. Hussaini, N.R. Dhumane, M.D. Shirsat, Synthesis of H2SO4 doped polyaniline film by potentiometric method, Bull. Mater. Sci. 29 (2006) 169–172, https://doi.org/10.1007/BF02704611.
[34] J.E.P. Da Silva, S.I.C. De Torresi, M.L.A. Temperini, Redox behavior of crosslinked polyaniline films, J. Braz. Chem. Soc. 11 (2000) 91–94, https://doi.org/10.1590/s0103-50532000000100016.
[35] Y.H. Yang, L. Bolling, M. Haile, J.C. Grunlan, Improving oxygen barrier and reducing moisture sensitivity of weak polyelectrolyte multilayer thin films with crosslinking, RSC Adv. 2 (2012) 12355–12363, https://doi.org/10.1039/c2ra21845c.
[36] J.W. Long, D.R. Rolison, Architectural design, interior decoration, and three-dimensional plumbing en route to multifunctional nanoarchitectures, Acc. Chem. Res. 40 (2007) 854–862, https://doi.org/10.1021/ar6000445.

[37] D. Jiang, X. Ma, Y. Fu, High-performance Sn-Ni alloy nanorod electrodes prepared by electrodeposition for lithium ion rechargeable batteries, J. Appl. Electrochem. 42 (2012) 555–559, https://doi.org/10.1007/s10800-012-0434-0.
[38] C. Wu, Q. Zhuang, S. Xu, Y. Cui, Y. Qiang, Z. Sun, Synthesis and characterization of α-Fe2O3/C composite anode for lithium ion batteries, Hua Hsueh Hsueh Pao 70 (2012) 51–57, https://doi.org/10.6023/A1106242.
[39] H.M. Zhang, X.M. Qin, H.Y. Sun, L.H. Liu, W. Li, Z.T. Lu, P.B. Han, Fabrication and electrochemical performance of Sn–Ni–Cu alloy films anode for lithium-ion batteries, J. Alloys Compd. 846 (2020), https://doi.org/10.1016/j.jallcom.2020.156322.